US ARMY
MATERIEL
COMMAND

MEMORANDUM REPORT BRL-MR-3447

COMPUTATIONAL SIMULATION OF TRANSONIC FLOW OVER PROJECTILE ROTATING BAND AND COMPARISON WITH EXPERIMENT

James E. Danberg
Karen R. Heavey
Miles C. Miller

May 1985

US ARMY BALLISTIC RESEARCH LABORATORY
ABERDEEN PROVING GROUND, MARYLAND

Destroy this report when it is no longer needed.
Do not return it to the originator.

Additional copies of this report may be obtained from the National Technical Information Service, U. S. Department of Commerce, Springfield, Virginia 22161.

The findings in this report are not to be construed as an official Department of the Army position, unless so designated by other authorized documents.

The use of trade names or manufacturers' names in this report does not constitute indorsement of any commercial product.

UNCLASSIFIED

SECURITY CLASSIFICATION OF THIS PAGE *(When Data Entered)*

REPORT DOCUMENTATION PAGE		READ INSTRUCTIONS BEFORE COMPLETING FORM
1. REPORT NUMBER MEMORANDUM REPORT BRL-MR-3447	2. GOVT ACCESSION NO.	3. RECIPIENT'S CATALOG NUMBER
4. TITLE *(and Subtitle)* COMPUTATIONAL SIMULATION OF TRANSONIC FLOW OVER PROJECTILE ROTATING BAND AND COMPARISON WITH EXPERIMENT		5. TYPE OF REPORT & PERIOD COVERED 6. PERFORMING ORG. REPORT NUMBER
7. AUTHOR(s) James E. Danberg* Karen R. Heavey Miles C. Miller**		8. CONTRACT OR GRANT NUMBER(s)
9. PERFORMING ORGANIZATION NAME AND ADDRESS US Army Ballistic Research Laboratory ATTN: AMXBR-LFD Aberdeen Proving Ground, Maryland 21005-5066		10. PROGRAM ELEMENT, PROJECT, TASK AREA & WORK UNIT NUMBERS RDT&E 1L162618AH80
11. CONTROLLING OFFICE NAME AND ADDRESS US Army Ballistic Research Laboratory ATTN: AMXBR-OD-ST Aberdeen Proving Ground, Maryland 21005-5066		12. REPORT DATE May 1985 13. NUMBER OF PAGES 44
14. MONITORING AGENCY NAME & ADDRESS *(if different from Controlling Office)*		15. SECURITY CLASS. *(of this report)* Unclassified 15a. DECLASSIFICATION/DOWNGRADING SCHEDULE

16. DISTRIBUTION STATEMENT *(of this Report)*

Approved for public release, distribution unlimited

17. DISTRIBUTION STATEMENT *(of the abstract entered in Block 20, if different from Report)*

18. SUPPLEMENTARY NOTES

*University of Delaware
Mechanical and Aerospace
Engineering Department
Newark, DE 19711

**US Army Armament, Munitions and Chemical
Command
Chemical Research and Development Center
Aberdeen Proving Ground, MD 21010

19. KEY WORDS *(Continue on reverse side if necessary and identify by block number)*

Projectile Rotating Band
Transonic Flow
Navier-Stokes
Pressure Distribution Data

20. ABSTRACT *(Continue on reverse side if necessary and identify by block number)*

An azimuthal-invarient Navier-Stokes computational method is used to predict the transonic (M = 0.94) flow field about an artillery shell with and without a simulated rotating band. The pressure distribution calculations at zero angle of attack are compared to wind tunnel data and reasonable agreement is obtained. Pressures on the boattail afterbody are slightly reduced when a rotating band is added. The computational results show this to be due to local flow separation. The projectile drag coefficient is predicted to increase by 9

DD FORM 1 JAN 73 1473 EDITION OF 1 NOV 65 IS OBSOLETE

UNCLASSIFIED

SECURITY CLASSIFICATION OF THIS PAGE *(When Data Entered)*

20. ABSTRACT (Continued)

percent because of the rotating band for the conditions considered in the calculation.

TABLE OF CONTENTS

LIST OF ILLUSTRATIONS

LIST OF TABLES

I. INTRODUCTION

A. Objective

The purpose of this report is to describe the results of the numerical computation of transonic flow over an ogive-cylinder-boattail projectile with a simulated rotating band. These computations are compared with the experimental data of Miller.[1] The experimental results obtained with the rotating band are also summarized.

B. Background

The rotating band is added to an artillery shell in order to impart stabilizing spin to the shell during launch. After launching, the surface protuberance of the band adds unwanted drag and can, through changes to the flow field, cause other effects on the aerodynamic characteristics. The transonic region is particularly important because most aerodynamic variables (drag, pitching moment, side force and Magnus moment) are usually at their maximum in this speed range and thus they are most sensitive to changes in configuration. A review has been made in Reference 2 of published information on rotating band aerodynamics and of some related data on protuberances and steps. It is concluded there that very little is understood about the magnitude of the effects caused by the addition of a rotating band in any speed range. For example, Figure 1 (which is taken from Reference 2) shows the considerable uncertainty regarding the rotating band drag. Although the band drag may only be of the order of 5 percent of the total drag of the projectile, the data cited in that figure show as much as a factor of two uncertainty in the rotating band drag coefficient at transonic speeds.

The primary effect of flow disturbances caused by the rotating band is to increase the pressure ahead of the band. This is because of the turning of the viscous layer which is followed by a series of expansion regions as the flow turns to move over the band. The flow then recompresses as it returns to the basic shell surface. This process is shown schematically in Figure 2. Actually some of these turning processes are caused by local separation and recirculation regions in front of and behind the band. These effects have been simulated in this work by introduction of ramp like surfaces ahead of and aft of the band in order to produce the strong pressure disturbances of the protuberance. If this can be shown to adequately reproduce the effects of the band, it would greatly simplfy the prediction of the aerodynamics of practical configurations.

The numerical solution technique employed here is the azimuthal-invariant unsteady, thin layer Navier-Stokes code which has been developed for

---

1. *M. C. Miller, "Wind Tunnel Measurements of the Magnus Induced Surface Pressures on a Spinning Projectile in Transonic Speed Range," AIAA Paper No. 83-1838, July 1983.*

2. *J. E. Danberg, "Numerical Modeling of Rotating Band Flow Field and Comparison with Experiment," U.S. Army Ballistic Research Laboratory, Aberdeen Proving Ground, Maryland, ARBRL-TR-02505, July 1983. (AD A131260)*

application to projectile shapes by Nietubicz, Pulliam and Steger.[3] The details of the equations used and of the method of obtaining solutions are described in the following sections along with the turbulence model employed.

II. EXPERIMENTAL DATA

A. Facilities and Test Conditions

The numerical results reported here are compared to the data obtained by Miller.[1] The main emphasis of his work was the measurement of pressures on a spinning projectile configuration. However,the primary interest here is the nonspinning case so that comparison with the numerical calculation is possible. The tests were performed in the NASA Ames Research Center 14-Foot Transonic Wind Tunnel on the projectile configuration defined in Figure 3. The conditions of these tests were Mach number of 0.94, a Reynolds number of 4×10^6 1/Ft. and angle of attack of 0, 4, 10°. The ogive-cylinder-boattail model was instrumented with 20 pressure taps; however, only three of these were on the rotating band. Figure 4 shows the location of all the taps. Tests were performed with and without the rotating band.

B. Configuration of the Rotating Band

The rotating band model afterbody which was constructed for these tests is shown in Figure 5. The dimensions were based on measurements obtained from a M549, 155 mm shell which was recovered after being fired. In this way the band was made to simulate the conditions in flight as accurately as possible. The crossection of the band is shown in Figure 5. Of the three pressure taps two were located on the land and one in the groove of the band.

III. AZIMUTHAL-INVARIANT THIN-LAYER NAVIER-STOKES CODE

A. Navier-Stokes Equations

The form of the Navier-Stokes solution technique employed here is the code developed by Nietubicz, et al[3] and applied to a number of projectile configurations as reported in References 4 and 5. The axisymmetric equations

---

3. *C. J. Nietubicz, C. J. Pulliam and J. L. Steger, "Numerical Solution of the Azimuthal-Invariant Thin Layer Navier-Stokes Equations," U. S. Army Ballistic Research Laboratory, Aberdeen Proving Ground, Maryland, ARBRL-TR-02227, March 1980. (AD A085716)*

4. *C. J. Nietubicz, "Navier-Stokes Computations for Conventional and Hollow Projectile Shapes at Transonic Velocities," U.S. Army Ballistic Research Laboratory, Aberdeen Proving Ground, Maryland, ARBRL-MR-03184, July 1982. (AD A116866)*

5. *C. J. Nietubicz, G. R. Inger and J. E. Danberg, "A Theoretical and Experimental Investigation of a Transonic Projectile Flow Field," U.S. Army Ballistic Research Laboratory, Aberdeen Proving Ground, Maryland, ARBRL-MR-03291, July 1983. (AD A131938)*

can be written in transformed body oriented coordinates and in nondimensional variables as:

$$\partial_\tau \hat{q} + \partial_\xi \hat{E} + \partial_\zeta \hat{G} + \hat{H} = Re^{-1}\, \partial_\zeta \hat{S} \tag{1}$$

where

$$\hat{q} = J^{-1} \begin{bmatrix} \overline{\rho} \\ \overline{\rho}\,\tilde{u} \\ \overline{\rho}\,\tilde{v} \\ \overline{\rho}\,\tilde{w} \end{bmatrix}$$

$$\hat{E} = \frac{U\hat{q}}{J} + \frac{\overline{p}}{J} \begin{bmatrix} 0 \\ \xi_x \\ \xi_y \\ \xi_z \\ U - \xi_\tau \end{bmatrix} \quad ; \quad \hat{G} = \frac{W\hat{q}}{J} + \frac{\overline{p}}{J} \begin{bmatrix} 0 \\ \zeta_x \\ \zeta_y \\ \zeta_z \\ W - \zeta_\tau \end{bmatrix}.$$

The countravariant velocities are:

$$\begin{aligned} U &= \xi_t + \xi_x\tilde{u} + \xi_y\tilde{v} + \xi_z\tilde{w} \\ V &= \eta_t + \eta_x\tilde{u} + \eta_y\tilde{v} + \eta_z\tilde{w} \\ W &= \zeta_t + \zeta_x\tilde{u} + \zeta_y\tilde{v} + \zeta_z\tilde{w} \end{aligned} \tag{2}$$

and the η-invariant source term can be written:

$$\hat{H} = J^{-1}\phi_\eta \begin{bmatrix} 0 \\ 0 \\ \rho V[R_\xi(U - \xi_t) + R_\zeta(W - \zeta_t)] \\ -\rho V R\phi_\eta(V - \eta_t) - \overline{p}/(R\phi_\eta) \\ 0 \end{bmatrix} \tag{3}$$

where R is the radius of the body and ϕ_η is a constant of proportionality between the circumferential angle and the transformed coordinate direction.

$$\hat{S} = J^{-1}(\mu + \mu_t)(\zeta_x^2 + \zeta_y^2 + \zeta_z^2) \begin{bmatrix} 0 \\ \tilde{u}_\zeta \\ \tilde{v}_\zeta \\ \tilde{w}_\zeta \\ 0.5(\tilde{u}^2 + \tilde{v}^2 + \tilde{w}^2)_\zeta + (a^2)_\zeta[(\gamma - 1)Pr_e] \end{bmatrix} \quad (4)$$

$$+ J^{-1} \left(\frac{\mu + \mu_t}{3}\right)(\zeta_x\tilde{u}_\zeta + \zeta_y\tilde{v}_\zeta + \zeta_z\tilde{w}_\zeta) \begin{bmatrix} 0 \\ \zeta_x \\ \zeta_y \\ \zeta_z \\ \zeta_x\tilde{u} + \zeta_y\tilde{v} + \zeta_z\tilde{w} \end{bmatrix}$$

These equations represent the time average turbulent flow equations in the following sense:

1. The velocities denoted with a tilde are mass-weighted time average quantities, i.e.,

$$\tilde{u} = \overline{\rho u}/\overline{\rho} \quad (5)$$

where the bar superscript refers to conventional time average.

2. The effective total Prandtl number is:

$$Pr_e = \frac{\overline{k} + k_t}{C_p(\overline{\mu} + \mu)} = \frac{\mu/Pr + \mu_t/Pr_t}{\overline{\mu} + \mu_t} \quad (6)$$

where k_t and μ_t are the eddy conductivity and eddy viscosity, respectively. Inherent in this form of the equations is the assumption of a Bousinesq formula for the time average Reynolds stresses.

3. The thin layer approximation has been applied after the transformation to body oriented coordinates so that only derivatives with respect to the "near" normal to the body coordinate (ζ) have been retained in the viscous terms.

4. The consistent equations of state which connect $\overline{e}$ in the energy equation with the mean pressure and temperature are:

$$\overline{p} = (\gamma - 1)[\,\overline{e} - 0.5\overline{\rho}(\tilde{u}^2 + \tilde{v}^2 + \tilde{w}^2)]$$

$$\overline{T} = \overline{p}/(\overline{\rho R}) \tag{7}$$

$$\overline{a^2} = \gamma\overline{RT}$$

where the turbulent kinetic energy has been neglected relative to the mean flow kinetic energy.

In the present non-spinning application of these equations, the body surface boundary condition becomes the adiabatic, no-slip condition. Problems caused by the singularity on the axis are avoided because the flux vectors there are zero by symmetry. Extrapolated outflow conditions are applied at the far stream boundary which includes an extended sting in order to avoid computation of the separated near wake flow field.

The equations are actually solved as finite difference equations written in delta form. An implicit approximate factorization scheme is employed.[6] The algorithm is second order in space with integration of the unsteady equations proceeding until steady state is achieved.

B. Turbulence Model

A two-layer algebraic turbulence model was employed to determine μ_t in these calculations. The model is due to Baldwin and Lomax.[7] For an attached boundary layer, the model can be described by the following equations:

1. Inner layer

$$\mu_t = \rho\ell^2\,|\omega| \tag{8}$$

---

6. *R. Beam and R. F. Warming, "An Implicit Factored Scheme for the Compressible Navier-Stokes Equations," AIAA Paper 77-645, June 1977.*

7. *B. S. Baldwin and H. Lomax, "Thin Layer Approximation and Algebraic Model for Separated Flows," AIAA Paper 78-257, January 1978.*

where

$$\ell = \kappa z[1 - \exp(-z^+/A^+)]$$

(z = normal to the surface in the untransformed coordinate, $z^+ = u_\tau z/\nu_w$, $A^+ = 26$). $|\omega|$ is the magnitude of the vorticity vector.

2. Outer layer

$$\mu_t = K\, C_{cp}\, \bar{\rho}\, F_{wake}\, F_{kleb} \tag{9}$$

where $F_{wake} = z_{max}F_{max}$ or $C_{wk}z_{max}\, U^2/F_{max}$ which ever is smallest. The quantities z_{max} and F_{max} are determined from the function:

$$F(z) = z|\omega|\ [1 - \exp(-z^+/A^+)] \tag{10}$$

where F_{max} is the maximum value of $F(z)$ and z_{max} is the value of z at which it occurs. The function $F_{kleb}(z)$ is the Klebanoff intermittency factor given by:

$$F_{kleb}(z) = [1 - 5.5\ (\frac{C_{kleb}z}{z_{max}})^6\ ]^{-1} \tag{11}$$

The quantity U is the maximum velocity in the profile for attached flow. The constants not already defined are: $K = 0.0168$, $C_{cp} = 1.6$, $C_{kleb} = 0.3$, $C_{wk} = 0.25$ and $\kappa = 0.4$.

C. Computational Model of the Rotating Band

Although in principle the Navier-Stokes code in the form employed here is capable of computing thin regions of separated flow, the method is far from routine. Thus a model rotating band configuration was employed which provides attached flow over a protuberance to simulate the flow above the dividing streamline; however, it does not account for the slip boundary condition on that streamline. Figure 6 shows the mathematical form used to define the geometry. The height of the band is $h/D = 0.0131$. The length of the quadratic ramps ahead of and behind the band are $L = 10h$ which corresponds, in at least a rough way, with the extent of the separated region. This model for the band is identical to that used at supersonic speeds as discussed in Reference 2.

D. Grid Generation

A modular, general purpose grid generation routine as described in Reference 8 was used to obtain a smoothly varying computational mesh. This method allowed arbitrary body geometry and investigator selected clustering of points near the band and other critical points on the body. Initial computations were performed using 90 longitudinal points on the model and 40 radial points. The number of points available on the rotating band was very limited which reduced the resolution in the region of rapidly varying flow. A new grid was selected, employing 125 points in the longitudinal direction with 100 on the 5.8 caliber model. Figure 7 shows an overall view of the grid system and Figure 8 shows a detail near the rotating band. There are 18 points on the band with 4 points each on the forward and rear ramps.

For the ogive nose region an elliptic grid generator has been employed. Straight lines normal to the axis of symmetry were used on the cylinder, rotating band and afterbody. An exponential stretching of points away from the model was used with the minimum spacing at the surface being 0.00002 diameter. The computational domain extends not less than four body lengths in all directions.

The one-half caliber boattail was terminated at 5.8 calibers corresponding to the physical model length and a constant diameter sting was continued from that point to the downstream boundary of the computational domain.

IV. RESULT

The numerical solution for the flow over the projectile permits the investigation of many details of the flow field which help explain the relatively few results which are obtained experimentally. The experiment of Miller provides surface pressure data at 20 points, only five of which are in the vicinity of the rotating band. On the other hand, the numerical solution is limited to a finite spacial resolution which affects the validity of the results. Thus the comparison of experimental and computational pressure distributions are used to establish the level of confidence in the computation. The examination of the various aspects of the numerical solution, e.g. Mach number contours, skin friction coefficients and velocity profiles gives understanding of the physical processes involved.

A. Pressure Coefficient Distribution

Figures 9 and 10 show the comparison of the numerical and experimental surface pressure coefficient distributions obtained at Mach number 0.94 with and without the rotating band. Figure 9 shows the comparison on the projectile without the band which indicates the overall capability of the numerical technique to predict the pressures. Figure 10 shows the comparison with the

---

8. *J. L. Steger, C. J. Nietubicz and K. R. Heavey, "A General Curvilinear Program for Projectile Configurations," U.S. Army Ballistic Research Laboratory, Aberdeen Proving Ground, Maryland, ARBRL-MR-03142, October 1981. (AD A107334)*

rotating band on the shell between x/D of 4.762 and 5.236 calibers. There is the expected rise in pressure ahead of the band followed by the expansion as the top of the band is reached. The data from the three taps on top of the band (C_p = -0.25) are in good agreement with the calculation. Behind the band, on the ramp of the numerical model, the computation predicts an extremely sharp expansion with a minimum C_p of about -0.65, followed by a recompression to a pressure corresponding to that observed ahead of the boattail without the band. The two pressure taps located in the region are slightly higher than that obtained numerically but of generally the correct level. From the start of the boattail at 5.3 calibers, the pressure distribution is somewhat more negative with the band than that obtained without it (see Figure 9). The quality of agreement between theory and experiment is essentially the same for both configurations. The total model length is 5.8 calibers and the relatively poor agreement of the last few points may be attributed to the sting like numerical model which is not a good representation of the base region flow field.

The comparison between computation and experiment in the case without the rotating band (Figure 9) shows generally good agreement with some discrepancy in the recompression region downstream of the ogive-cylinder junction and on the boattail. These discrepancies, of the order of 8 percent in pressure are probably due to grid resolution of the expansion and subsequent shock wave. An overall improvement in the representation of these regions was obtained by increasing the number of longitudinal grid points from 90 to 125. The region near the base is poorly predicted again because of the sting model.

As a general conclusion it may be said that the experimental pressure distribution is fairly accurately described by the numerical model with some qualifications in regions of minimum pressure. Unfortunately no pressure taps were located in the expansion region just behind the rotating band so that no conclusion regarding the adequacy of the flow field modeling in that location is possible.

B. Mach Contours

Figure 11 shows the calculated Mach contours for the rotating band case. The supersonic pockets just after the ogive-cylinder junction and behind the rotating band-start of the boattail are clearly evident. Both of these regions are terminated by shock waves of comparible strength. Apparently, the subsonic compression region ahead of the band involves relatively small increases in Mach number and pressure as compared to the effect of the same surface change in supersonic flow.[1,2] The recompression just downstream of the rotating band, apparent from the pressure distribution, does not show up as a shock wave or as a pocket of significantly decreased Mach number. The Mach number appears to remain supersonic throughout the region until the boattail recompression shock wave just ahead of the base.

C. Skin Friction Coefficient

Figure 12 shows the skin friction distribution obtained from the numerical solution. Five major spikes are observed related to five regions of high pressure expansion.

1. Near x/D = 0.0; this is the expansion created by the hemispherical nose cap-ogive junction which forms the numerical approximation to the blunt nosed projectile.

2. x/D = 3; the junction of the ogive and cylinder.

3. x/D = 4.9; at the leading edge of the top of the rotating band. The local minimum ahead of this peak is attributable to the compression ramp of the model band.

4. x/D = 5.1; the rear of the band which is followed by a minimum due to the recompression on the ramp and the short downstream cylindrical element.

5. x/D = 5.3; the expansion at the boattail junction.

One significant unexpected result is the negative skin friction obtained on the boattail which suggests separated flow at the boattail shock wave. The configuration without the rotating band shows a very low C_f in this region but no negative values. This shows the potentially important downstream effect of the rotating band which could cause some change in the boattail drag and could explain why the rotating band minimum pressure in this region is lower than the corresponding value for the no rotating band case. However, since the experimental pressure distribution does not agree with the prediction, it is uncertain whether or not separation is induced by the band in the experiment.

D. Velocity Profiles

Although the numerical model of the rotating band is not physically correct because it does not properly describe the separated flow regions near the surface, the strong pressure gradients provide a severe test of the turbulence model. Figures 13 and 14 show the development of the velocity profiles. The curve labeled x/D = 4.61 on the first figure corresponds to a point just at the begining of the ramp. Curves labeled 4.76 and 4.85 are on the compression surface and show relatively little change. Curve 4.92 is on the top of the band and 5.00 is on the centerline. Both show considerable acceleration of the flow in the viscous layer and a pronounced overshoot at the outer edge of the boundary layer. Curves 5.04 and 5.08 of Figure 14 continue the development on top of the band and 5.15, 5.24 and 5.22 are on the downstream ramp. Curve 5.15 is just off the top of the band and shows the very strong local acceleration experienced by the flow. The subsequent points show the spreading of the viscous region as the flow begins to relax back toward the constant pressure region on the short cylinder before the boattail. Consistent with the Mach number contour plots, the regions away from the surface show an almost monotonic increase in velocity as the flow moves over the rotating band. The boundary layer becomes thinner in the expansion regions with strong overshoots in velocity near the edge of the layer.

E. Effect of Rotating Band on Overall Aerodynamic Characteristics

The previous sections have described the insight gained from the flow field computation at zero angle of attack and zero spin rate. It is particularly desirable to consider the effect of the rotating band on overall

aerodynamic parameters which determine the shell performance. Although the calculations have not been performed at angle of attack or with spin it is possible to use the zero angle of attack calculations to help explain the experimental results obtained from the NASA Ames tests. Table 1 provides a summary of the integrated data obtained with and without the rotating band. Four properties are considered: normal force, pitching moment, side force, and Magnus moment all in terms of nondimensional coefficients. These data were obtained by integrating the measured pressure distributions and are broken down in terms of the contribution from the ogive nose, the cylindrical centerbody and the afterbody. The rotating band pressure distribution is included in the cylindrical contribution. The normal force and pitching moment are considered to show the effects of angle of attack and that spin has only a higher order effect on these characteristics. On the other hand, the side force and moment are essentially asymmetric effects created by the spin of the projectile at angle of attack. Figure 15 defines the coordinate system employed with these forces and moments.

1. Normal Force and Moment. The computed pressure distribution at zero angle of attack shows that the pressure increases ahead of the band and decreases behind in roughly the same amount so that relatively little direct effect is anticipated on normal force. However, the negative pressure coefficient region is considerably reduced and thus the asymmetries at angle of attack which give rise to the negative boattail lift are also reduced. This is born out by the data in Table 1. The decrease in negative lift on the boattail in the amount of 20 percent produces an overall increase in the C_{N_α} of about 3.6 percent for this configuration. The moment coefficient is affected in a similar amount but opposite sign. Thus a decrease in the negative lift of the boattail results in a decrease in the de-stabilizing moment in the net amount of 4.6 percent.

2. Magnus Force and Moment. Magnus effects may be expected to be sensitive to large gradients in the surface pressure distribution as well as the magnitude of the pressures. The addition, the rotating band creates very severe pressure gradients with the result that the side force on the cylinder is significantly increased. However, the decrease in pressure on the boattail produces a compensating effect on the afterbody so that the overall change in side force is of the order of 1.7 percent. On the other hand, the location of these forces produces a significant 13.5 percent decrease in the overall Magnus moment coefficient.

As an additional check on these experimental results, the data are compared in Table 2 with the data reported by Platou and Nielsen in Reference 9. The C_{y_p} and C_{n_p} results from integrating the pressure distribution are in excellent agreement with those obtained from direct wind tunnel force and moment balance tests.

---

9. *A. S. Platou and G. I. T. Nielsen, "Some Aerodynamic Characteristics of the Artillery Projectile XM549," U.S. Army Ballistic Research Laboratory, Aberdeen Proving Ground, Maryland, ARBRL-MR-2284, April 1973. (AD 910093L)*

3. Rotating Band Drag Coefficient. Under the assumption that the numerical prediction of the pressure distribution is at least approximately correct despite the limitations in the model, it is possible to estimate the drag of the band itself by assuming that the maximum pressure acts on the forward face of the band and that the minimum pressure acts on the rear face. Thus the change in the drag coefficient due to the band is:

$$\Delta C_{D_{RB}} = 4(C_{p_{max}} - C_{p_{min}})h/D$$

which in this case is approximately $\Delta C_D = 0.017$. Integration of the pressure over the boattail results in an increase in C_D in the amount:

$$\Delta C_{D_{BT}} = 0.005.$$

Giving a net increase in drag coefficient of 0.022 or about 9 percent of the total drag (assuming $C_D = 0.25$) neglecting any change in the base drag.

V. SUMMARY AND CONCLUSIONS

This report describes the results of applying an azimuthal-invariant Navier-Stokes computational technique to predict the flow field about an artillery shell flying at Mach number of 0.94. The results are compared to experimentally measured pressure distributions obtained by Miller[1] in the NASA Ames Research Center transonic wind tunnel.

The numerical technique is essentially that developed by Nietubicz, et al[2] which includes the Baldwin-Lomax turbulence model. In order to avoid computing separated flow regions ahead of and behind the rotating band, the recirculating regions were simulated by quadratic ramps of length equal to 10 band heights before and behind the actual bands.

The presence of the band produces a significant change in the pressure distribution with a high pressure region on the upstream ramp. This is followed by an extremely short expansion zone where the pressure falls to a level corresponding to supersonic flow on top of the band. The resulting pressure agrees with those obtained experimentally although the computation did not include the details of the lands and grooves of the experimental rotating band configuration.

The pressure tap locations in the experiment were not placed so as to confirm or contradict the existence of a second sharp expansion which occurs just downstream of the rotating band. The numerical prediction shows a drop in pressure coefficient immediately behind the band, followed by a recompression on the aft ramp to about the same level as on top of the band and consistent with the pressure obtained just ahead of the cylinder-boattail junction without the band. The pressure on the boattail appears to be only slightly

modified, but small changes can have significant effects on the projectile drag. The boattail contributes an important fraction of the total drag at transonic speeds.

The reason for the decreased pressure on the boattail is attributed to flow separation at the boattail shock wave. This separation region is observed in the skin friction distribution which is not observed in the calculations without the band.

The experimental results regarding the overall aerodynamic coefficients of the shell can be interpreted by considering the numerical solution even though the current numerical results apply only to zero angle of attack and zero spin. The change in boattail pressure distribution because of the rotating band induced separation, results in slightly increased normal force coefficients at angle of attack and a decrease in pitching moment. This is consistent with a reduced negative lift on the boattail attributed to separation.

The band induced change in the side force is negligible but this is due to a compensating decrease in boattail contribution matching an increase on the cylinder because of the rotating band. The Magnus moment is the most significantly affected quantity. The experimental data indicate a 13.5 percent decrease because of the band.

The numerical pressure data were used to estimate the change in drag coefficient caused by the rotating band. The estimated C_D is increased by slightly less than 7 percent due to the pressure acting directly on the band. The decreased pressure on the boattail also increases the drag by about 2 percent so that the total increase in drag is 9 percent under the conditions considered in this report.

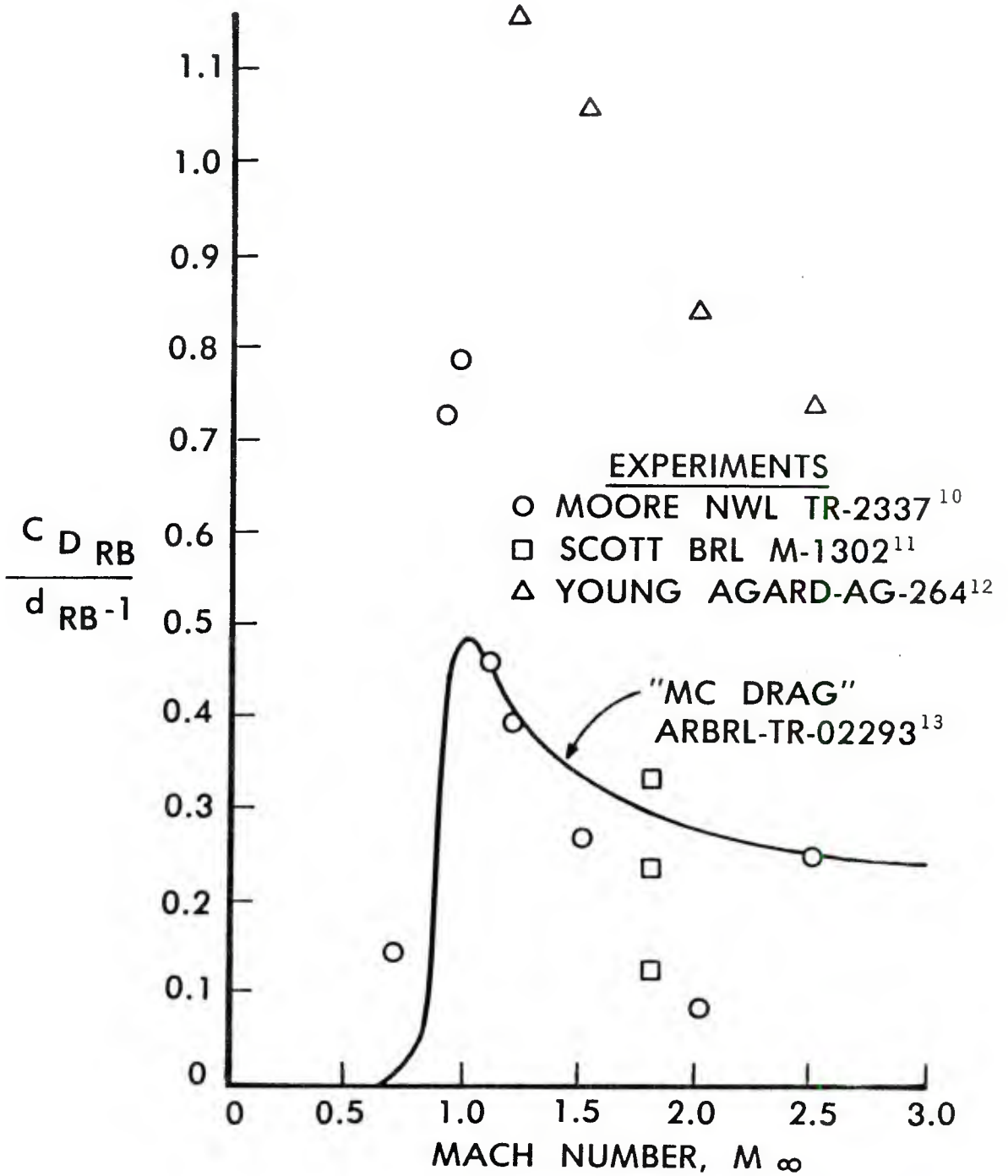

Figure 1. Rotating Band Drag Coefficient

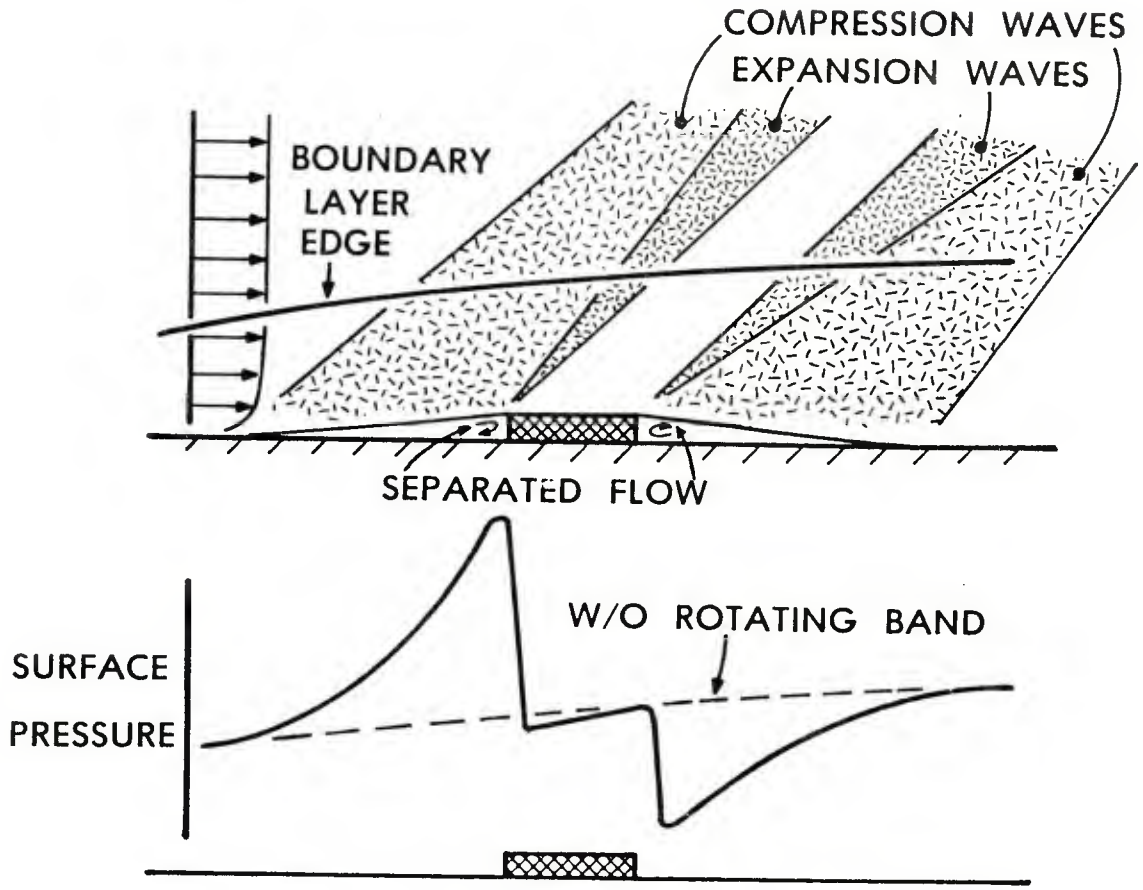

Figure 2. Rotating Band Flow Field

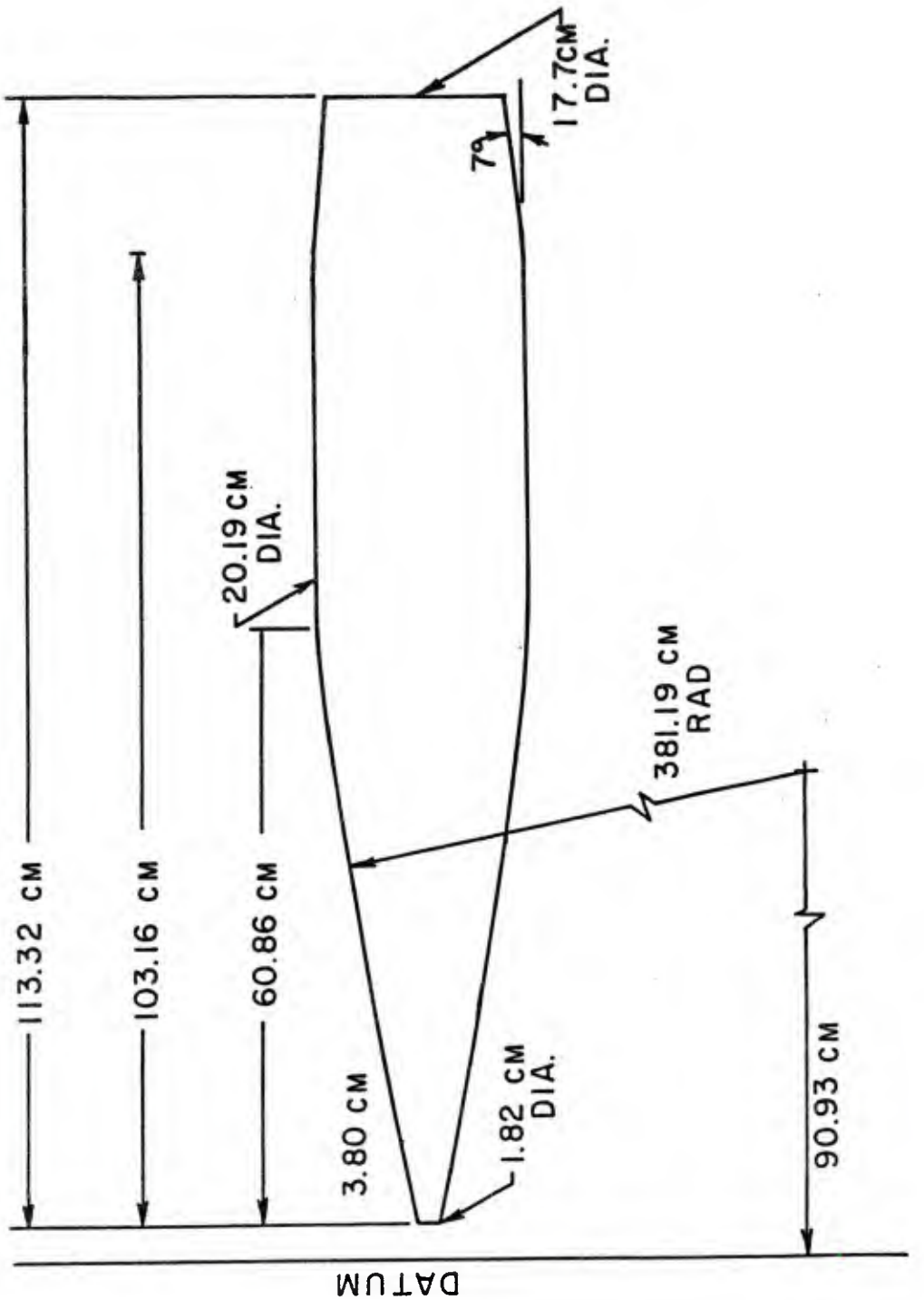

Figure 3. Conical Boattail Model Configuration Showing Dimensions

TAP NO.	TAP LOCATION Z (IN.)	Z/L	Z/d	Y (IN.)	Y (Y/d)	(-) DEG	TAP LOCATION NOTES	TAP CIRCUMFERENTIAL LOCATION WRT MAIN TAPS (DEG)
1	22.449	.503	2.824	3.875	.487	4.5	OGIVE	0
2	23.450	.526	2.950	3.969	.499	4.5		30
3	23.961	.537	3.014	3.975	.5	0	OGIVE/CYLINDER JUNCTION CYLINDER	0
4	24.461	.548	3.077	3.975	.5	0		30
5	25.461	.571	3.203	3.975	.5	0		0
6	27.461	.615	3.454	3.975	.5	0		
7	29.461	.660	3.706	3.975	.5	0		
8	31.461	.705	3.957	3.975	.5	0		
9	33.461	.750	4.209	3.975	.5	0		
10	37.821	.848	4.757	3.975	.5	0	ROTATING BAND	0
11	38.321	.859	4.820	3.975	.5	0		30
12	38.821	.870	4.883	3.975	.5	0		0
13	39.616	.888	4.983	3.975	.5	0	CYLINDER	30
14	40.116	.899	5.046	3.975	.5	0		0
15	40.616	.910	5.109	3.975	.5	0	CYLINDER/BOATTAIL JUNCTION BOATTAIL	30
16	41.151	.922	5.176	3.938	.495	7.0		0
17	42.159	.945	5.303	3.813	.425	7.0		0
18	43.236	.969	5.438	3.688	.480	7.0		30
19	43.725	.980	5.500	3.625	.456	7.0		0
20	44.616	.994	5.578	2.750	.346	90°	BASE	90

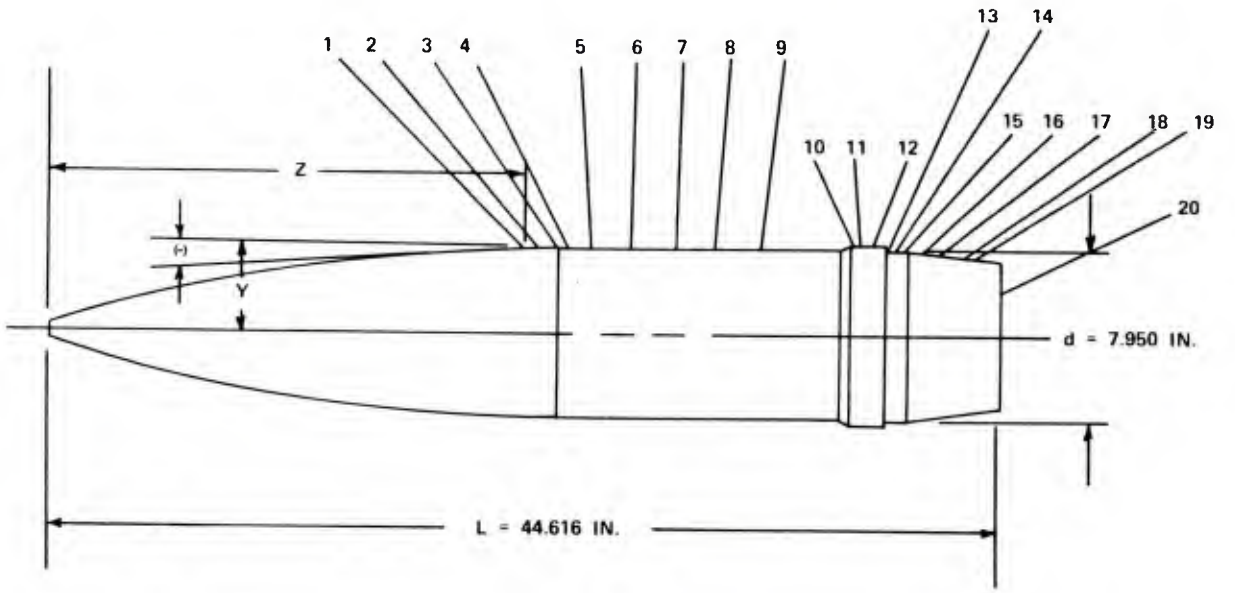

Figure 4. Pressure Tap Locations

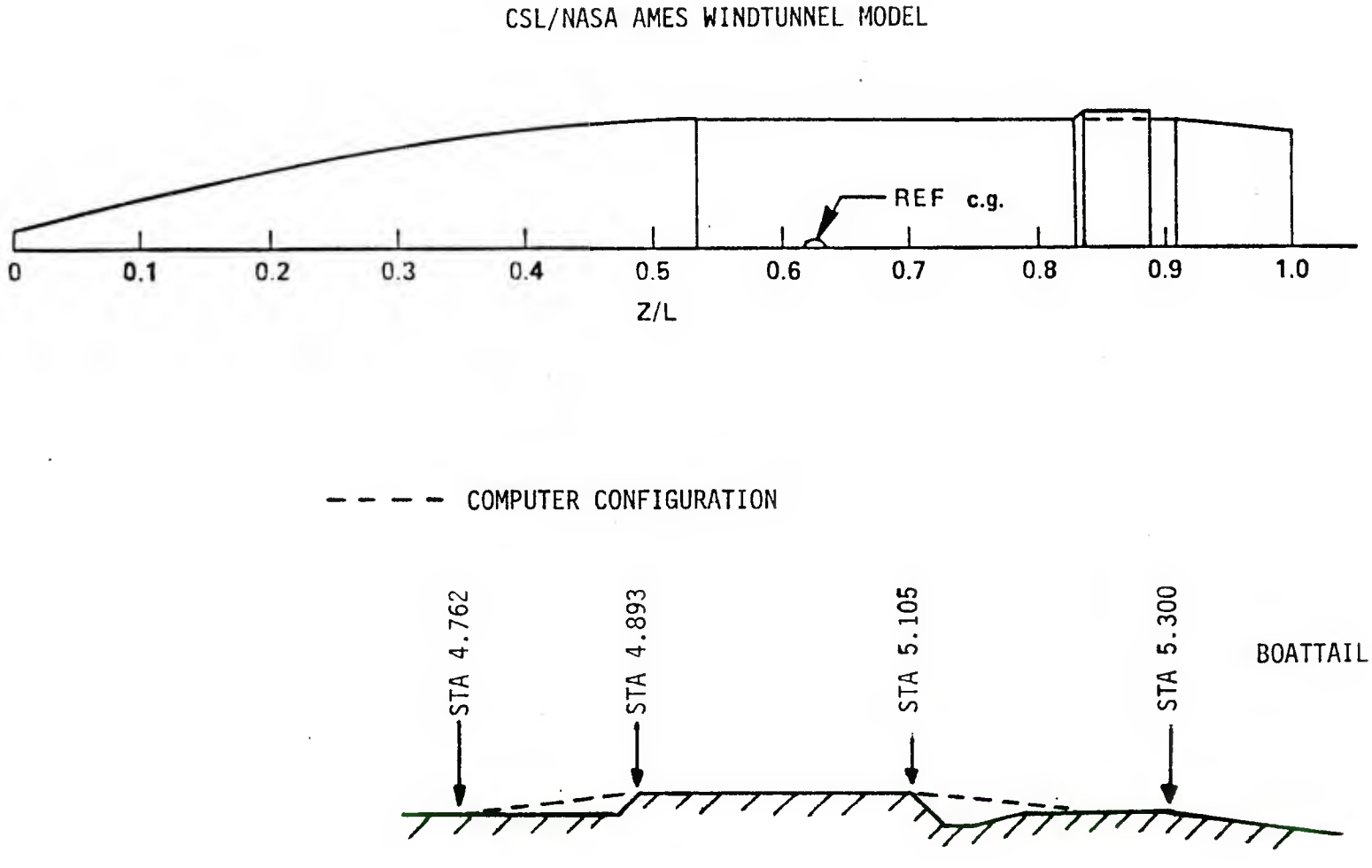

Figure 5. Rotating Band Configuration

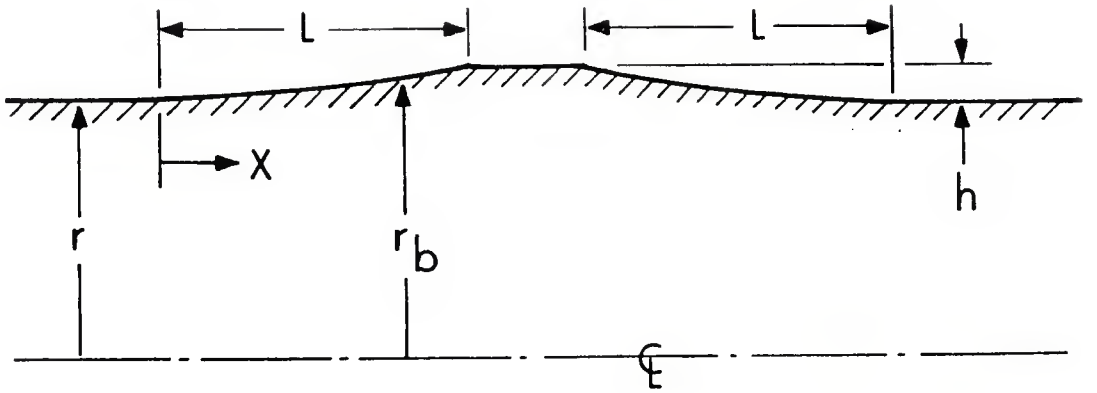

$$r_b = r + h\ f_n(X/L)$$

$$f_n(X/L) = \begin{cases} (X/L)^2 \\ 1 - \cos\left(\frac{\pi}{2}\ \frac{X}{L}\right) \end{cases}$$

NEGLECTS SLIP BOUNDARY CONDITION ON DIVIDING STREAMLINE

Figure 6. Rotating Band Numerical Model

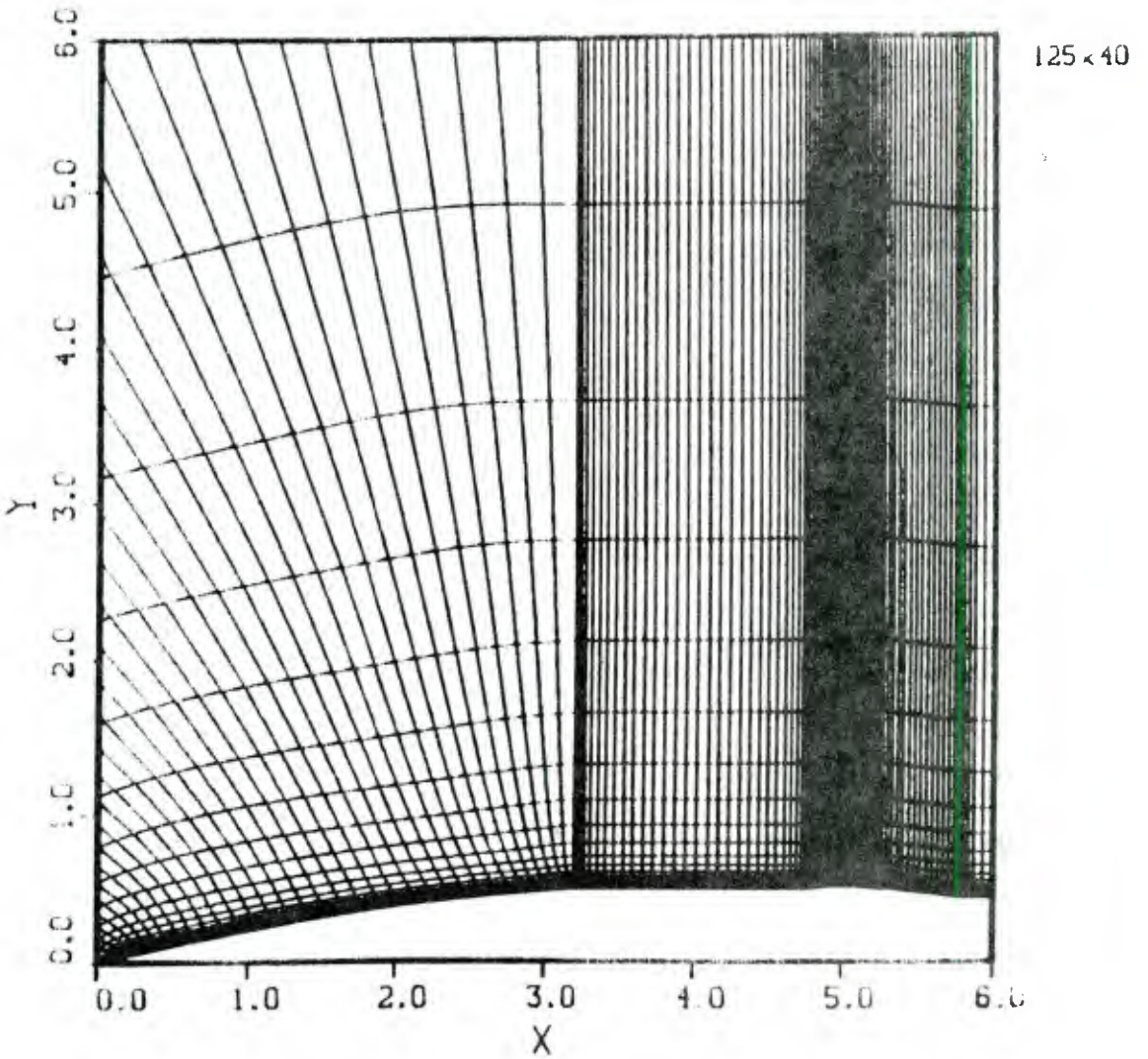

Figure 7. Compuational Grid for Rotating Band Calculation

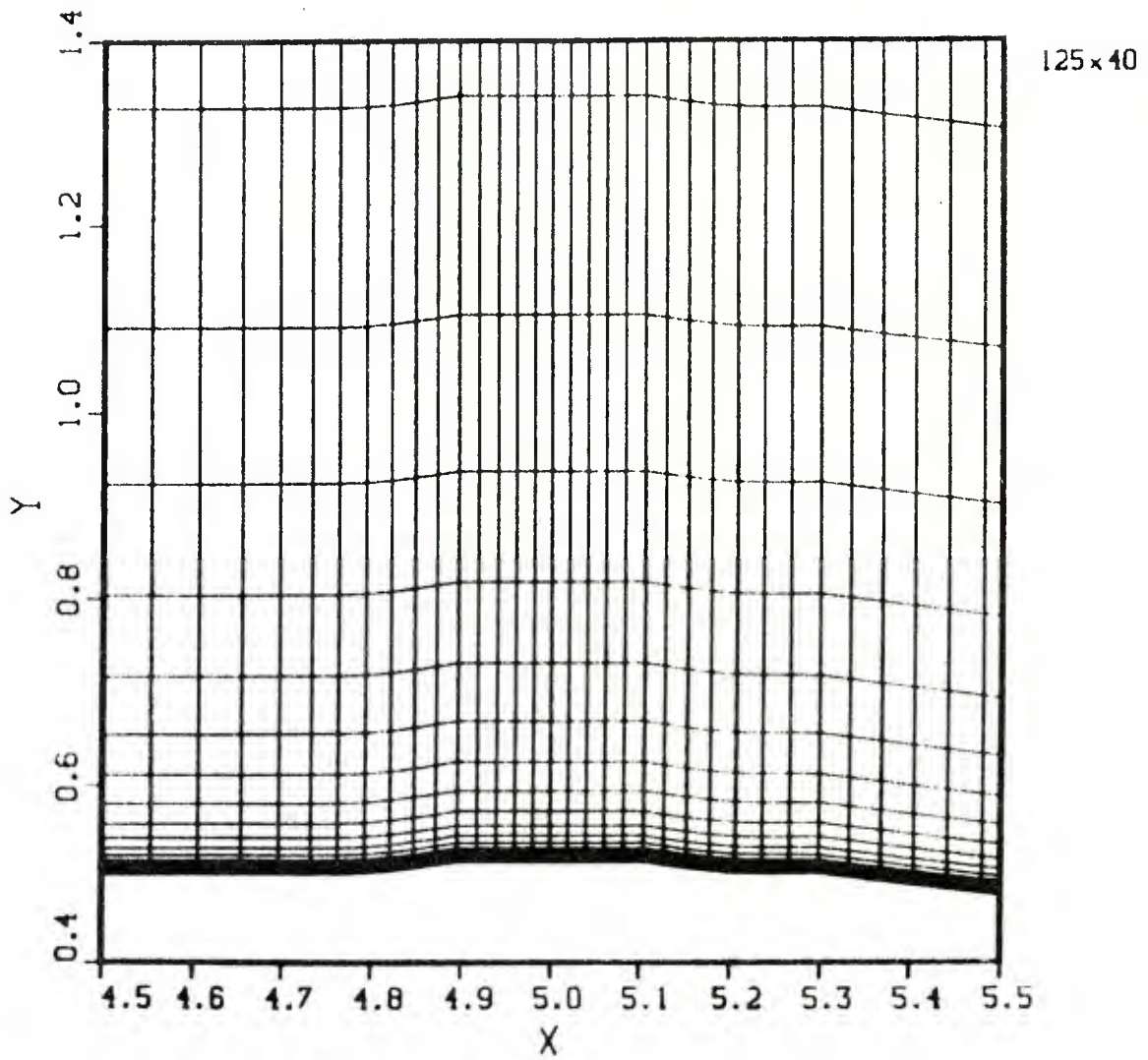

Figure 8. Detail of Grid in Vicinity of Rotating Band

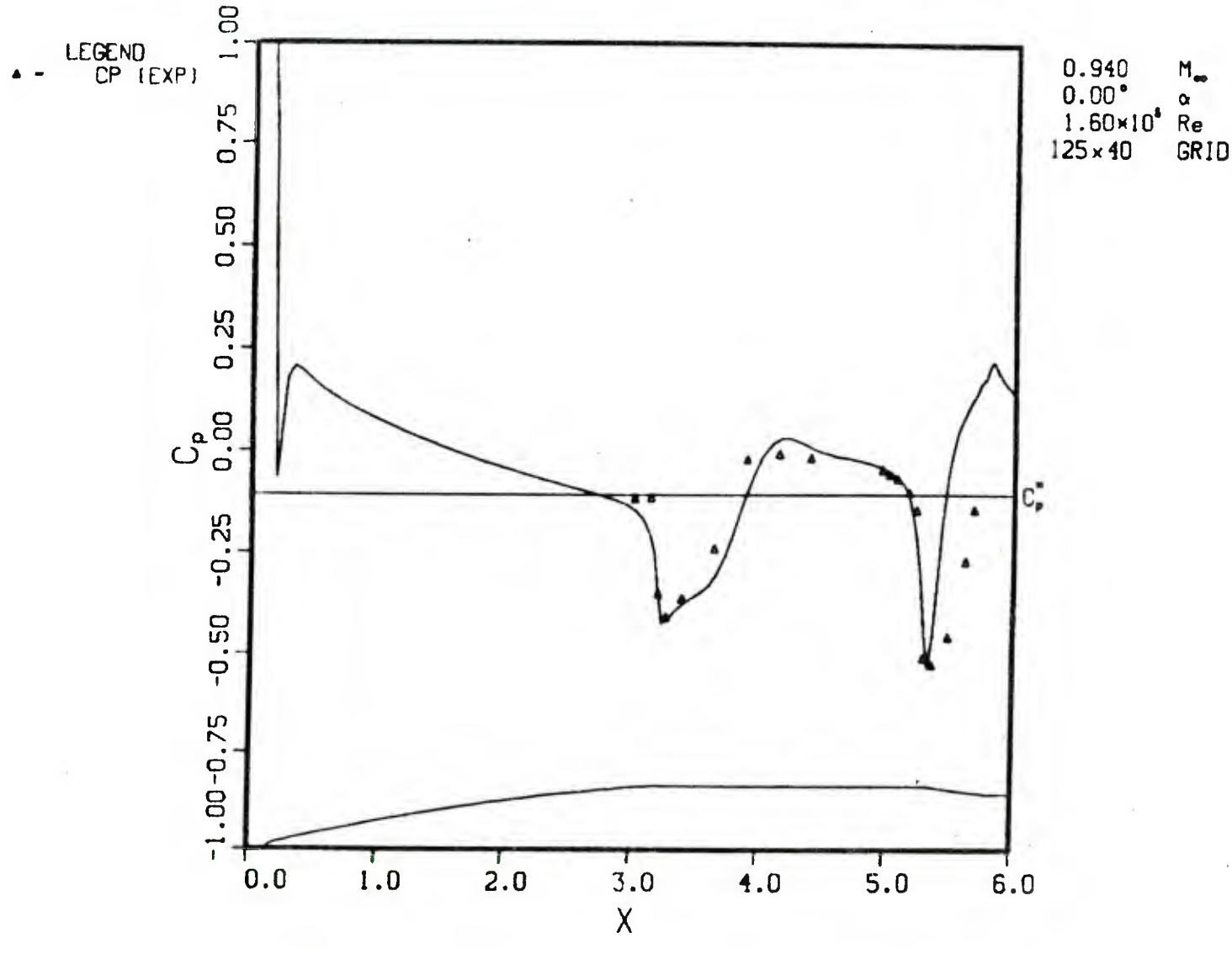

Figure 9. Pressure Coefficient Distribution on Model without Rotating Band and Comparison with Experiment

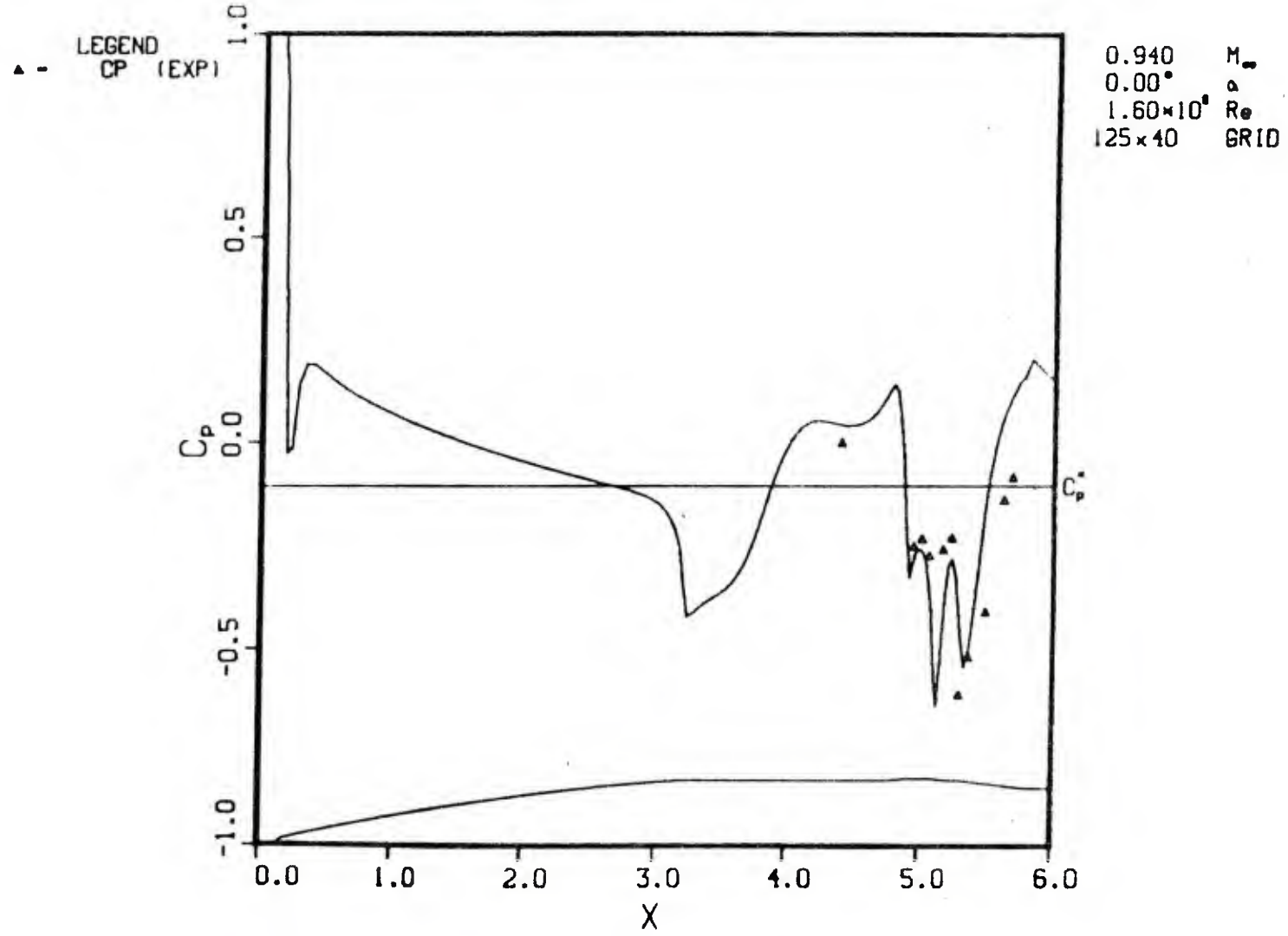

Figure 10. Pressure Coefficient Distribution on Model with Rotating Band and Comparison with Experiment

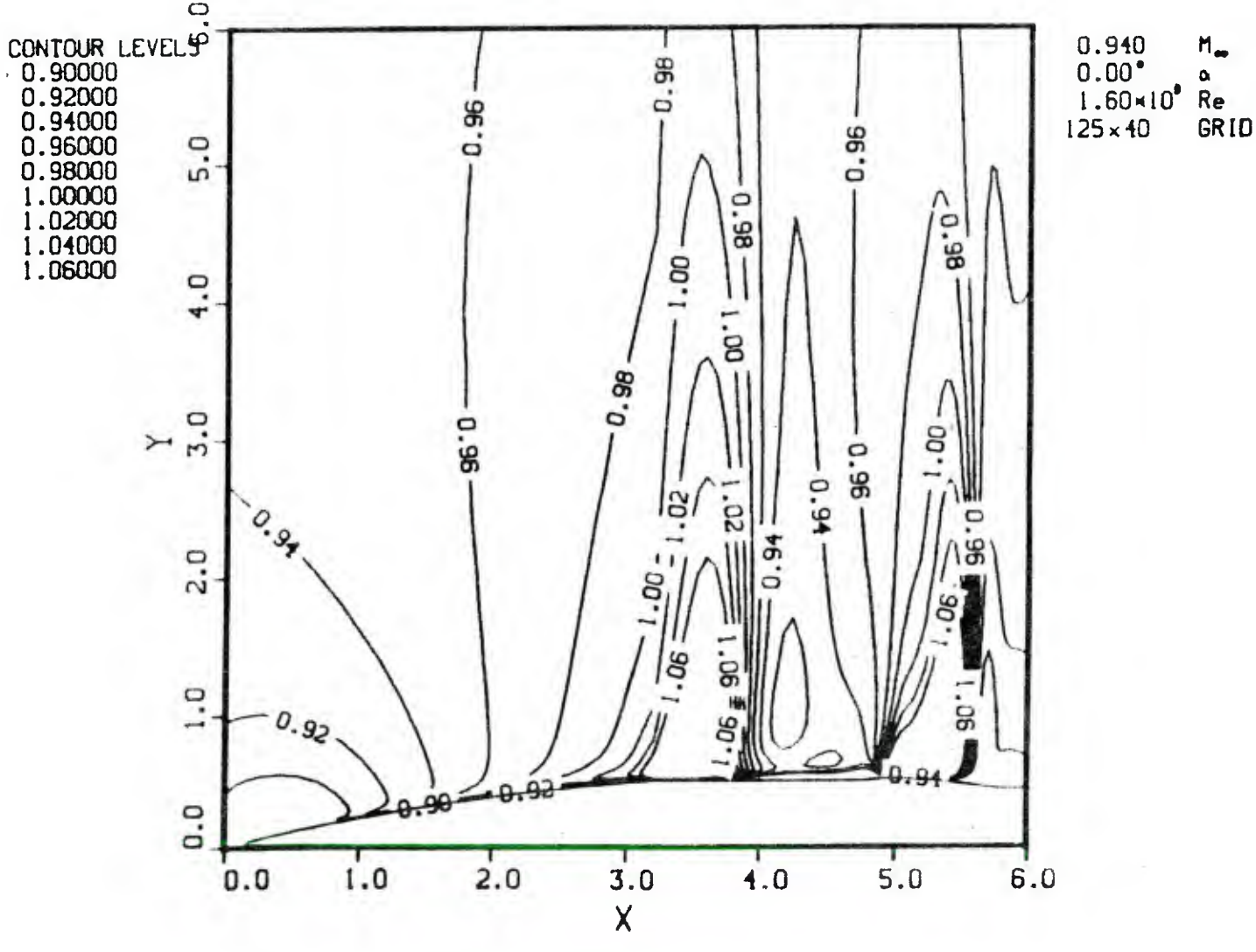

Figure 11. Mach Number Contours

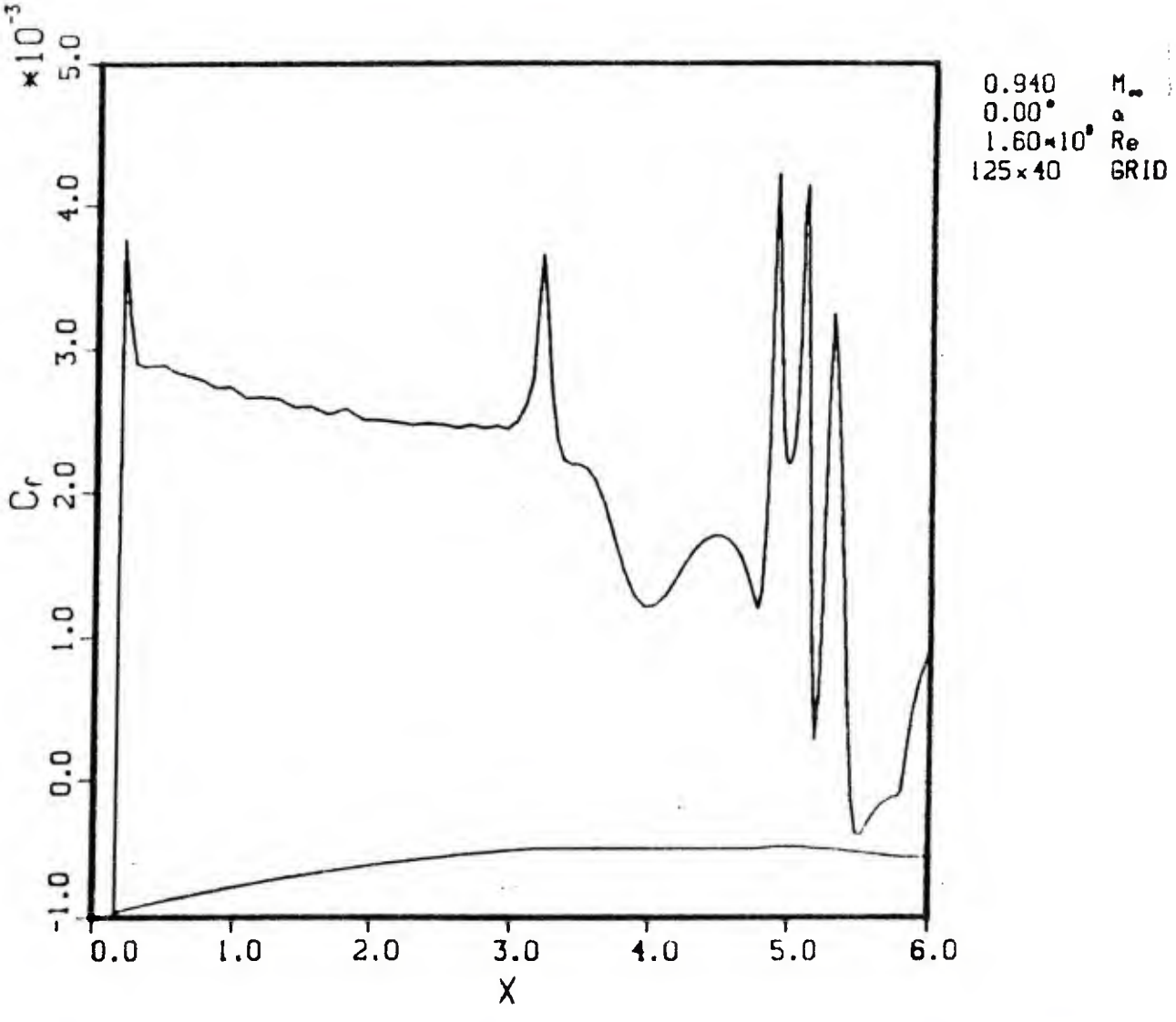

Figure 12. Skin Friction Coefficient Distribution, Rotating Band Model

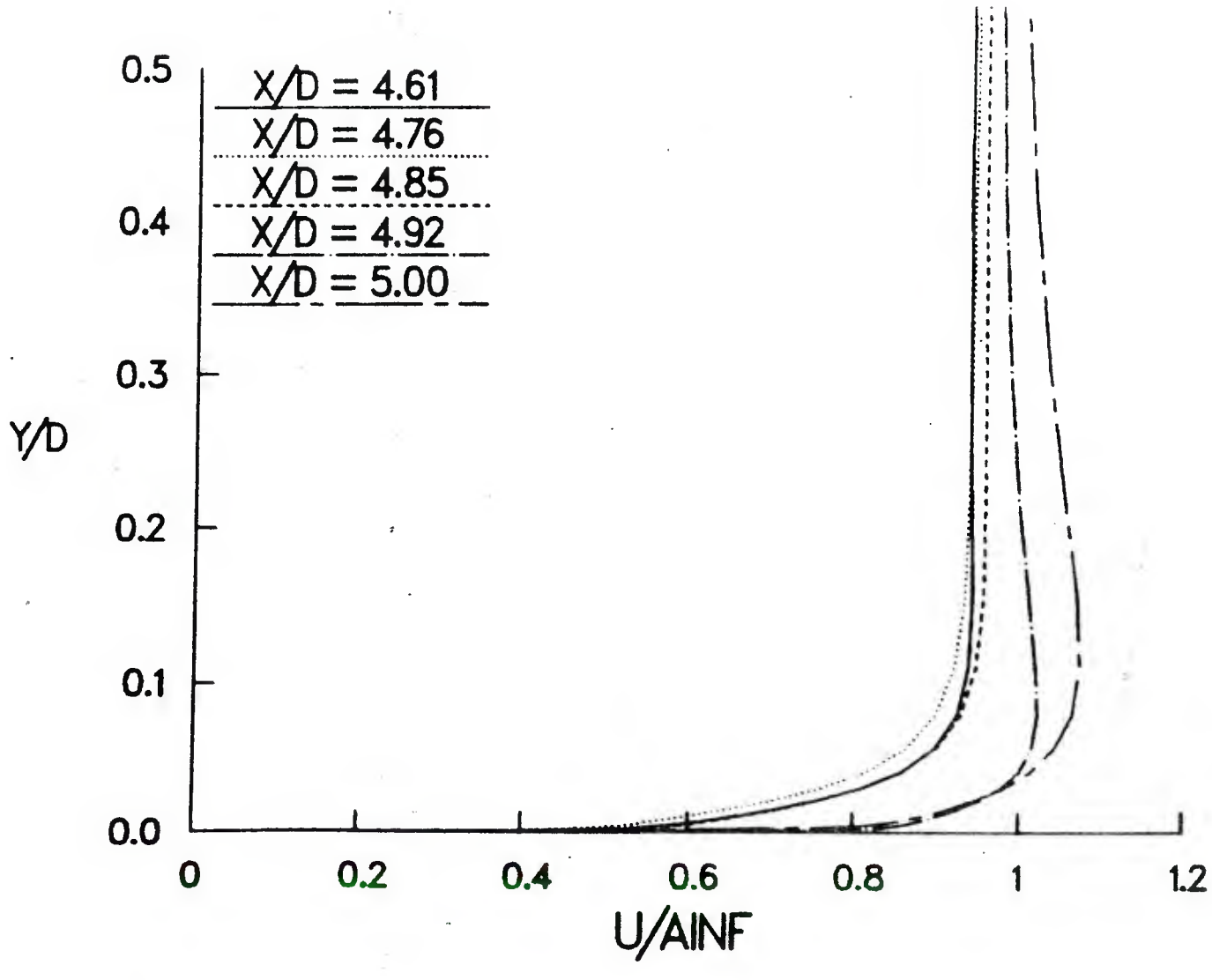

Figure 13. Velocity Profiles in the Vicinity of the Rotating Band (Forward Half of Band)

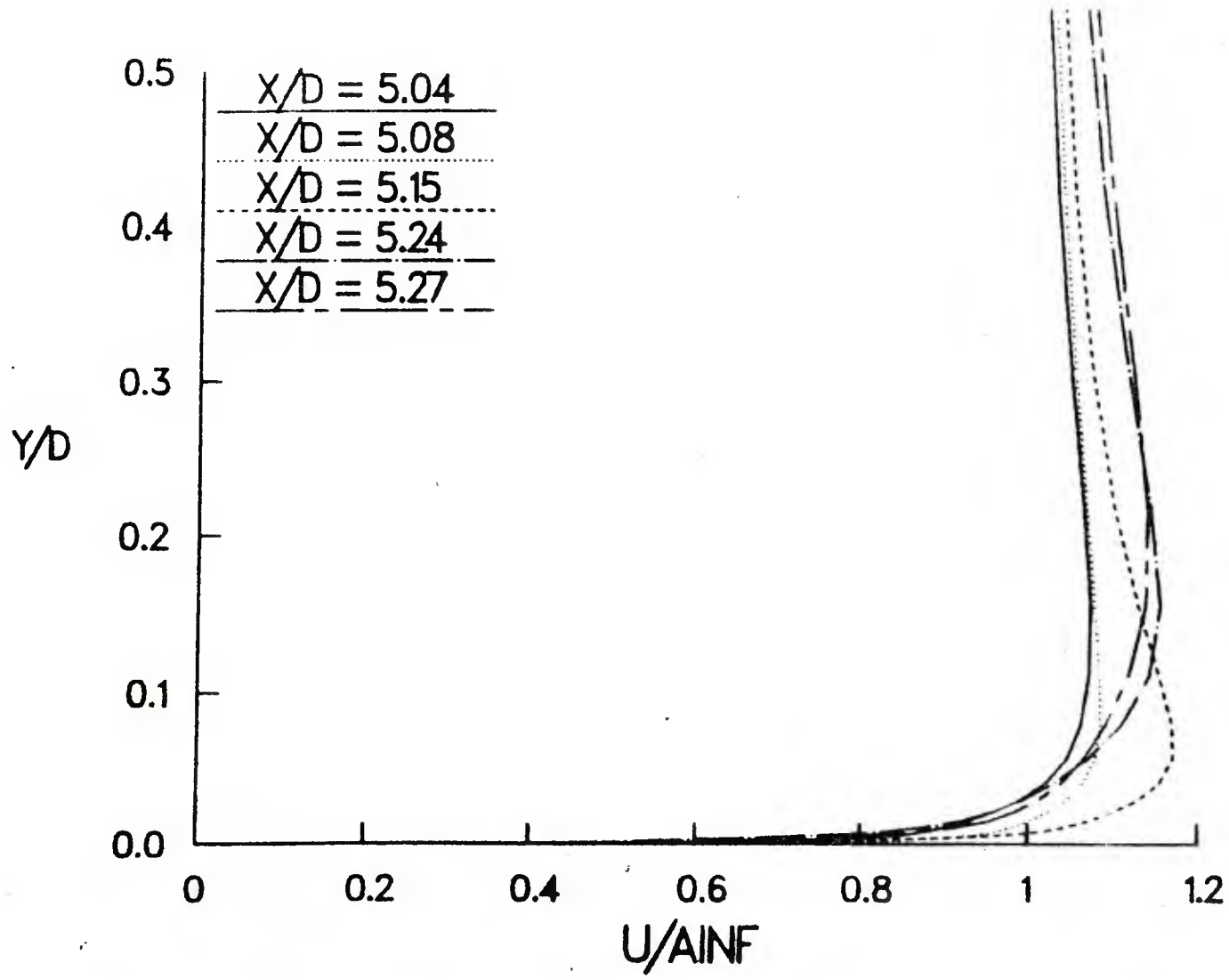

Figure 14. Velocity Profiles in Vicinity of the Rotating Band (Aft Half of Band)

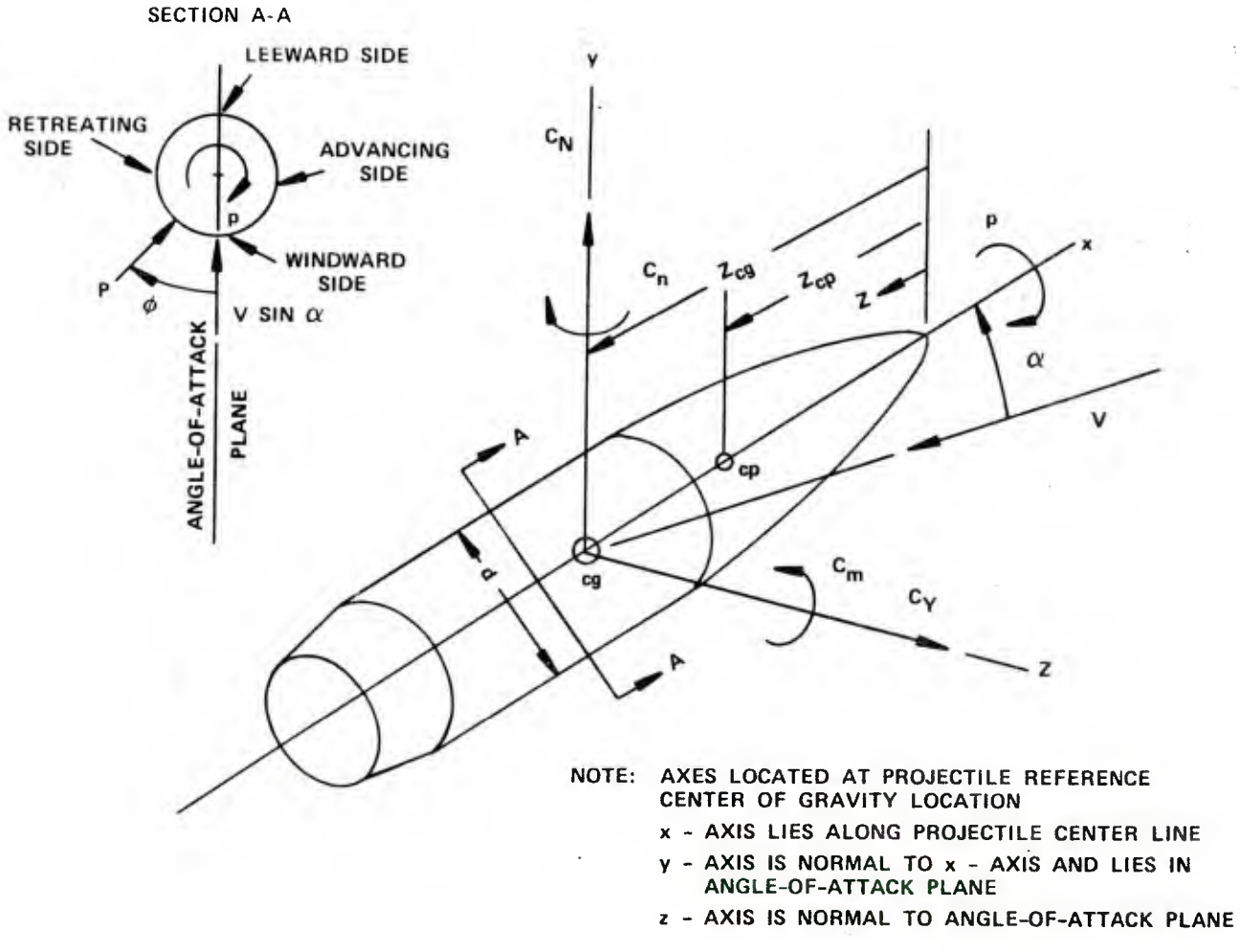

Figure 15. Coordinate System for Forces and Moments

Table 1. Aerodynamic Coefficients Based on Integration of the Measured Pressure Distribution

MODEL CONFIGURATION:

8 INCH DIAMETER MODEL
3 CALIBER OGIVE
2 CALIBER CYLINDER
5 CAL BOATTAIL
REF c.g. AT Z/L = .625

TEST CONDITION:

MACH .94
$\alpha = 10^{o}$
$R_d = 4 \times 10^6$/FT
p = -4900 RPM
$\hat{p} = -.162$

TERM	ROTATING BAND OFF	ROTATING BAND ON
C_{N_α} (OGIVE)	1.94	1.95
C_{N_α} (CYLINDER)	.60	.62
C_{N_α} (BOATTAIL)	-.31	-.25
C_{N_α} (TOTAL)	2.24	2.32
C_{m_α} (OGIVE)	3.47	3.47
C_{m_α} (CYLINDER)	-.36	-.39
C_{m_α} (BOATTAIL)	.60	.46
C_{m_α} (TOTAL)	3.71	3.54
$Z_{cp/L}$	.33	.35
C_{Y_p} (OGIVE)	−.004	−.004
C_{Y_p} (CYLINDER)	−.092	−.149
C_{Y_p} (BOATTAIL)	−.080	−.026
C_{Y_p} (TOTAL)	−.176	−.179
C_{n_p} (OGIVE)	−.003	−.003
C_{n_p} (CYLINDER)	.063	−.139
C_{n_p} (BOATTAIL)	.148	.043
C_{n_p} (TOTAL)	.208	.180
$Z_{cp/L}$ (MAGNUS)	.836	.804

Table 2. Comparison of Aerodynamic Coefficients from Two Experiments

TERM	INTEGRATION OF SURFACE PRESSURE DATA	DIRECT FORCE AND MOMENT DATA, REF: BRLMR 2284
	$\alpha = 10°$	
C_{Y_p} (TOTAL)	-.179	-.175
C_{n_p} (TOTAL)	.180	.180
	$\alpha = 4°$	
C_{Y_p} (TOTAL)	-.104	-.090
C_{n_p} (TOTAL)	.090	.085

Test Conditions

$M_\infty = 0.94$

$pd/2V = 0.164$

Rotating Band On

REFERENCES

1. M. C. Miller, "Wind Tunnel Measurements of the Magnus Induced Surface Pressures on a Spinning Projectile in Transonic Speed Range," AIAA Paper No. 83-1838, July 1983.

2. J. E. Danberg, "Numerical Modeling of Rotating Band Flow Field and Comparison with Experiment," U.S. Army Ballistic Research Laboratory, Aberdeen Proving Ground, Maryland, ARBRL-TR-02505, July 1983. (AD A131260)

3. C. J. Nietubicz, C. J. Pulliam and J. L. Steger, "Numerical Solution of the Azimuthal-Invariant Thin Layer Navier-Stokes Equations," U.S. Army Ballistic Research Laboratory, Aberdeen Proving Ground, Maryland, ARBRL-TR-02227, March 1980. (AD A085716)

4. C. J. Nietubicz, "Navier-Stokes Computations for Conventional and Hollow Projectile Shapes at Transonic Velocities," U.S. Army Ballistic Research Laboratory, Aberdeen Proving Ground, Maryland, ARBRL-MR-03184, July 1982. (AD A116866).

5. C. J. Nietubicz, G. R. Inger and J. E. Danberg, "A Theoretical and Experimental Investigation of a Transonic Projectile Flow Field," U.S. Army Ballistic Research Laboratory, Aberdeen Proving Ground, Maryland, ARBRL-MR-03291, July 1983. (AD A131938)

6. R. Beam and R. F. Warming, "An Implicit Factored Scheme for the Compressible Navier-Stokes Equations," AIAA Paper 77-645, June 1977.

7. B. S. Baldwin and H. Lomax, "Thin Layer Approximation and Algebraic Model for Separated Flows," AIAA Paper 78-257, January 1978.

8. J. L. Steger, C. J. Nietubicz and K. R. Heavey, "A General Curvilinear Program for Projectile Configurations," U.S. Army Ballistic Research Laboratory, Aberdeen Proving Ground, Maryland, ARBRL-MR-03142, October 1981. (AD A107334)

9. A. S. Platou and G. I. T. Nielsen, "Some Aerodynamic Characteristics of the Artillery Projectile XM549," U.S. Army Ballistic Research Laboratory, Aberdeen Proving Ground, Maryland, ARBRL-MR-2284, April 1973. (AD 910093L)

10. F. G. Moore, "A Study to Optimize the Aeroballistic Design of Naval Projectiles," NWL TR-2337, September 1969.

11. W. E. Scott, "The effect of Rotating Band Upon Some Aerodynamic Coefficients of the Seven Caliber Army-Navy Spinner Rocket at Mach 1.8", U.S. Army Ballistic Research Laboratory, Aberdeen Proving Ground, Maryland, ARBRL-MR-1302, September 1960. (AD 246223)

12. A. D. Young, and J. H. Patterson, "Aircraft Excrescence Drag," AGARDograph No. 264, July 1981.

13. R. L. McCoy, "'MCDRAG' - A Computer Program for Estimating the Drag Coefficients of Projectiles," U.S. Army Ballistic Research Laboratory, Aberdeen Proving Ground, Maryland, ARBRL-TR-02293, February 1981. (AD A098110)

LIST OF SYMBOLS

$\overline{a^2}$	time average of the velocity of sound squared
C_D	drag coefficient (based on projectile cross sectional area)
C_p	pressure coefficient
c_p	specific heat at constant pressure
C_{N_α}	derivative of the normal force coefficient with respect to angle of attack
C_{n_p}	derivative of Magnus moment coefficient with respect to spin rate
C_{m_α}	derivative of pitching moment coefficient with respect to angle of attack
C_{y_p}	derivative of side force coefficient with respect to spin rate
D	body diameter
d_{RB}	rotating band diameter in calibers
e	energy
$\hat{E},\hat{G},\hat{H},\hat{S}$	flux vectors of transformed Navier-Stokes equation
h	height of rotating band
J	transformation Jacobian
$\overline{k}$	molecular thermal conductivity
k_t	turbulent eddy thermal conductivity
L	body length
ℓ	Prandtl mixing length
M_∞	free stream Mach number
Pr	Prandtl number
Pr_e	effective Prandtl number (see Equation 6)
Pr_t	turbulent Prandtl number = $k_t/(c_p \mu_t)$
$\overline{p}$	time average pressure

$\hat{q}$ flux vector of dependent variables in the transformed Navier-Stokes equations

R radius of the body in η-invariant Navier-Stokes equations

$\overline{R}$ gas constant

r radius of the body

r_b radius of body with rotating band

U,V,W contravariant velocity components

$\tilde{u},\tilde{v},\tilde{w}$ mass-weighted time average velocity components

u_τ shear velocity

Greek Symbols

α angle of attack

γ ratio of specific heats

κ universal constant in Prandtl mixing length equation

$\overline{\mu}$ molecular viscosity

μ_t turbulent eddy viscosity

ξ,η,ζ transformation coordinates in axial, circumferential and radial directions

$\overline{\rho}$ time averaged density

τ transformed time

ϕ circumferential angle

ν_w kinematic viscosity evaluated at the body surface

ω vorticity

Subscripts

RB rotating band

BT boattail

t turbulent

e	effective
∞	free stream conditions

Superscripts

—	time average
~	mass-weighted time average (see Equation 5)

DISTRIBUTION LIST

No. of Copies	Organization
12	Administrator Defense Technical Info Center ATTN: DTIC-DDA Cameron Station Alexandria, VA 22304-6145
1	HQDA DAMA-ART-M Washington, DC 20310
1	Commander US Army Materiel Command ATTN: AMCDRA-ST 5001 Eisenhower Avenue Alexandria, VA 22333-0001
8	Commander Armament R&D Center US Army AMCCOM ATTN: SMCAR-TDC SMCAR-TSS SMCAR-LCA-F Mr. D. Mertz Mr. E. Falkowski Mr. A. Loeb Mr. R. Kline Mr. S. Kahn Mr. H. Hudgins Dover, NJ 07801
1	Commander US Army Armament, Munitions and Chemical Command ATTN: SMCAR-ESP-L Rock Island, IL 61299
1	Director Benet Weapons Laboratory Armament R&D Center US Army AMCCOM ATTN: SMCAR-LCB-TL Watervliet, NY 12189
1	Commander US Army Aviation Research and Development Command ATTN: AMSAV-E 4300 Goodfellow Blvd St. Louis, MO 63120

No. of Copies	Organization
1	Director US Army Air Mobility Research and Development Laboratory Ames Research Center Moffett Field, CA 94035
1	Commander US Army Communications - Electronics Command ATTN: AMSEL-ED Fort Monmouth, NJ 07703
1	Commander US Army Electronics Research and Development Command Technical Support Activity ATTN: DELSD-L Fort Monmouth, NJ 07703-5301
3	Commander US Army Missile Command ATTN: AMSMI-R AMSMI-RDK Dr. Bill Walker Mr. R. Deep Redstone Arsenal, AL 35898
1	Commander US Army Missile Command ATTN: AMSMI-YDL Redstone Arsenal, AL 35898
1	Commander US Army Tank Automotive Command ATTN: AMSTA-TSL Warren, MI 48090
1	Director US Army TRADOC Systems Analysis Activity ATTN: ATAA-SL White Sands Missile Range, NM 88002
1	Commander US Army Research Office Durham P. O. Box 12211 Research Triangle Park, NC 27709-2211

DISTRIBUTION LIST

No. of Copies	Organization
1	Commander US Naval Air Systems Command ATTN: AIR-604 Washington, D. C. 20360
2	Commander David W. Taylor Naval Ship Research and Development Center ATTN: Dr. S. de los Santos Mr. Stanley Gottlieb Bethesda, Maryland 20084
2	Commander US Naval Surface Weapons Center ATTN: Code DK20 Dr. F. Moore Dahlgren, VA 22448
1	Commander US Naval Surface Weapons Center ATTN: Dr. U. Jettmar Silver Spring, MD 20910
1	Commander US Naval Weapons Center ATTN: Code 3431, Tech Lib China Lake, CA 93555
1	Commander US Army Development & Employment Agency ATTN: MODE-TED-SAB Fort Lewis, WA 98433
1	Director NASA Langley Research Center ATTN: NS-185, Tech Lib Langley Station Hampton, VA 23365
1	Commandant US Army Infantry School ATTN: ATSH-CD-CSO-OR Fort Benning, GA 31905
1	AFWL/SUL Kirtland AFB, NM 87117
3	Sandia National Laboratory ATTN: Technical Staff, Dr. W.L. Oberkampf Aeroballistics Division 5631, H.R. Vaughn Dr. F. Blottner Albuquerque, NM 87184
1	Massachusetts Institute of Technology ATTN: Tech Library 77 Massachusetts Avenue Cambridge, MA 02139
1	Virginia Polytechnic Institute & State University ATTN: Dr. Clark H. Lewis Department of Aerospace & Ocean Engineering Blacksburg, VA 24061
1	University of Delaware Mechanical and Aerospace Engineering Department ATTN: Dr. J. E. Danberg Newark, DE 19711

Aberdeen Proving Ground

Dir, USAMSAA
ATTN: AMXSY-D
AMXSY-MP, H. Cohen

Cdr, USATECOM
ATTN: AMSTE-TO-F

Cdr, CRDC, AMCCOM,
ATTN: SMCCR-RSP-A
SMCCR-MU
SMCCR-SPS-IL
Miles C. Miller,
SMCCR-RSP-A

USER EVALUATION SHEET/CHANGE OF ADDRESS

This Laboratory undertakes a continuing effort to improve the quality of the reports it publishes. Your comments/answers to the items/questions below will aid us in our efforts.

1. BRL Report Number _____ Date of Report _____

2. Date Report Received _____

3. Does this report satisfy a need? (Comment on purpose, related project, or other area of interest for which the report will be used.) _____

_____

_____

4. How specifically, is the report being used? (Information source, design data, procedure, source of ideas, etc.) _____

_____

_____

5. Has the information in this report led to any quantitative savings as far as man-hours or dollars saved, operating costs avoided or efficiencies achieved, etc? If so, please elaborate. _____

_____

_____

6. General Comments. What do you think should be changed to improve future reports? (Indicate changes to organization, technical content, format, etc.)

_____

_____

_____

CURRENT ADDRESS

_____
Name

_____
Organization

_____
Address

_____
City, State, Zip

7. If indicating a Change of Address or Address Correction, please provide the New or Correct Address in Block 6 above and the Old or Incorrect address below.

OLD ADDRESS

_____
Name

_____
Organization

_____
Address

_____
City, State, Zip

(Remove this sheet along the perforation, fold as indicated, staple or tape closed, and mail.)